Bull. Min. Res. Exp. (2018) 156: 247-258

Bulletin of the Mineral Research and Exploration

http://bulletin.mta.gov.tr

The Naşa intrusion (Western Anatolia) and its tectonic implication: A joint analyses of gravity and earthquake catalog data

C. Ertan TOKER[a]*, Emin U. ULUGERGERLİ[b] and Ali R. KILIÇ[c]

[a]*Department of Geophysical Researches, General Directorate of Mineral Research and Exploration, Ankara, Turkey. orcid org/0000-0002-4923-9835*
[b]*Çanakkale Onsekiz Mart University, Geophysic Department Çanakkale. orcid.org/0000-0001-5639-1109*
[c]*Department of Geophysical Researches, General Directorate of Mineral Research and Exploration, Ankara, Turkey. orcid 0000-0002-2127-249X*

Research Article

Keywords:
Gravity, Earthquake, Simav, Graben, edge detection, Euler deconvolution.

ABSTRACT

The gravity data gathered in and around the Simav Graben in Western Anatolia were reprocessed and reinterpreted by using the standard deviation filter and the Euler deconvolution. The joint evaluation of results from the interpretation of gravity data and seismological studies indicates the presence of new intrusive structures in the vicinity of Simav. The intrusion is located in the eastern margin of the graben and has a thickness of 12-15 km at 2.5-3 km depth below the surface. Numerous earthquakes recorded in the eastern part of the graben are associated with this intrusion. Besides, the multi-dimensional modelling study of the gravity data allowed us to display the Simav Graben, the fold of the Simav Fault, the intrusion named as Naşa, and the epicenters of earthquake within the same tectonic frame. All tectonic structures were marked on the three dimensional relief model.

Received Date: 21.10.2016
Accepted Date: 28.09.2017

1. Introduction

It is important to understand the boundaries of geological structures and tectonic discontinuities while exploring the subsurface. In this context, when processing the geophysical data, especially those gathered from the gravity method, it is aimed to clarify the geological setting by increasing the resolution of structural elements and tectonic components and to be contributed to tectonic and geodynamic interpretations. The number of the data processing software and filter applications suggested to obtain much clear and meaningful boundaries are increasing steadily. These filters, also known as the edge detector, produce successful results when they are applied to synthetic data either as single or sequentially. However, the applications on real data show that there is still a need for new techniques (Arısoy and Dikmen, 2013; Cooper, 2013; Zhou et al., 2013).

The Simav Graben, which is one of the West Anatolian grabens, has become subject to many investigations in order to demarcate the intra-graben structure and margins of the basin. Some of the previous studies used seismological data to explain the mechanism of the Simav Fault, which forms the graben boundary, and the causation of earthquakes (Bekler et al., 2011; Toker, 2014; Gündoğdu et al., 2016; Kartal and Kadiroğlu, 2014). In addition, the components of tectonic structures and their formation mechanisms were investigated by evaluating the focal distribution geometry of earthquakes in the graben.

The gravity data of the Simav Graben were evaluated by both the conventional approach (Demirbaş and Uslu, 1984) and imaging techniques (Toker, 2014). The moving standard deviation (MSD) filter can be an example to imaging techniques. In previous studies, the usage of an MSD filter with a fixed window size of 2x2 of which its sensitivity cannot be adjusted because of the window dimension, was suggested as an image processing filter (Jassim, 2013). However in this study, the "moving standard deviation with variable dimension" (MSDVD) filter

* *Corresponding author: C. Ertan TOKER, toker.ertan@gmail.com*
http://dx.doi.org/10.19076/mta.346159

was applied to the potential field data. The processed data were interpreted in order to infer new geological and tectonic information.

The purpose of boundary detection methods is to enhance the variations in data. To do that; first the derivatives in different degrees are calculated, then new images are obtained either from the combination or ratios (phase) of these derivatives. The analytical signal and vertical derivative (Miller and Singh, 1994) methods can be given as examples to such image enhancement processes. The second vertical derivative of the analytical signal (Hsu et al, 1996), the total horizontal derivative of tilt angle (Verdusco et al., 2004), the hyperbolic tilt angle, the second vertical derivative of the hyperbolic tilt angle (Cooper and Cowan, 2004) and the analytical signal obtained from the tilt angle (Ansari and Alamdar, 2011) were utilized in previous studies. The MSD filter was previously compared with Sobel and Kany filters as the edge detector in image processing (Jassim, 2013). In this study, it was demonstrated that the MSDVD filter could also be used in detecting the boundaries of geological structures.

2. Method

The results that are obtained from the application of MSDVD on to data will be examined. The sensitivity of the filter depends on the window size and can be changed optionally. The most important characteristic of this process, which is a kind of image enhancement technique, is that it does not require any sort of derivative or phase calculation. In this respect, it differs from derivative and phase filters. This laterally sensitive filter uses data statistic and produces structurally enhanced information in the output. In the following sections, first we will present the results obtained by application of filter both on the synthetic and Simav data. Later on; we will produce images, which show boundaries of the geological units, and relief map of the study area by using three dimensional standard Euler deconvolution, then assess the elements of emerging geological structures.

2.1. Conceptual Model Application

İn generally the standard deviation is given in the following formula as;

$$\sigma = ((\sum(x)^2 - n*x^2)/(n-1))^{1/2} \quad (1)$$

The equation calculates the variations of "x" variables from n sequential observations around the mean value. The input "x" is an array and contains the measurements along a line. If "x" contains two dimensional variables then standard deviations are calculated by moving the weighted filter windows in k x k window size. The weight values are obtained from deviations off the mean value over data windows. By selecting the "k" index the window size and sensitivity can be adjusted.

In order to obtain a symmetric filter, the k should be set as positive and integer number.

In generally "windowed moving standard deviation" given as;

$$M = \text{movstd}(Amxn,k) \quad (2)$$

returns an array of local k-point standard deviation values. Each standard deviation is calculated over a sliding window of length k across neighboring elements of A (https://www.mathworks.com/help/matlab/ref/std.html).

$$\text{Filter windows} = (2*k+1, 2*k+1) \quad (3)$$

In equation (3), the filter dimensions will be 3,3 for k=1. Similarly; the filter will be 5,5 for k=2. This filter is centered by moving for each elements of the data and standard deviations are calculated over the data grid. By means of weighted and filtered value assigned to the filter center the numerical array representing the structural elements are obtained. Along the edges of data array, the filter is applied by reducing its size (Cooper and Cowan, 2008).

Synthetic data are produced for the model given in figure 1a. The results of 3x3 MSDVD and 5x5 MSDVD are seen in figures 1 b) and 1 c), respectively. In the case of increased "k", it is seen that the anomaly of the horizontal, long prism located at the central part becomes stronger and the structure gains weight (Figure 1 c). Anomalies of the prisms get widens towards the inner edges of the structures. In the map of 2^{nd} vertical derivatives given in figure 1 d), the structure boundaries are enhanced depending on the derivation direction. The values of the 2^{nd} vertical derivative vary between +20 and -15 mgal/km. Despite that, the range in figure 1 b) varies between 0 and +45 mgal and presents much stable variations. Figure 1e shows the horizontal gradient which is similar to figure 1 b). However, it is obtained by derivatives.

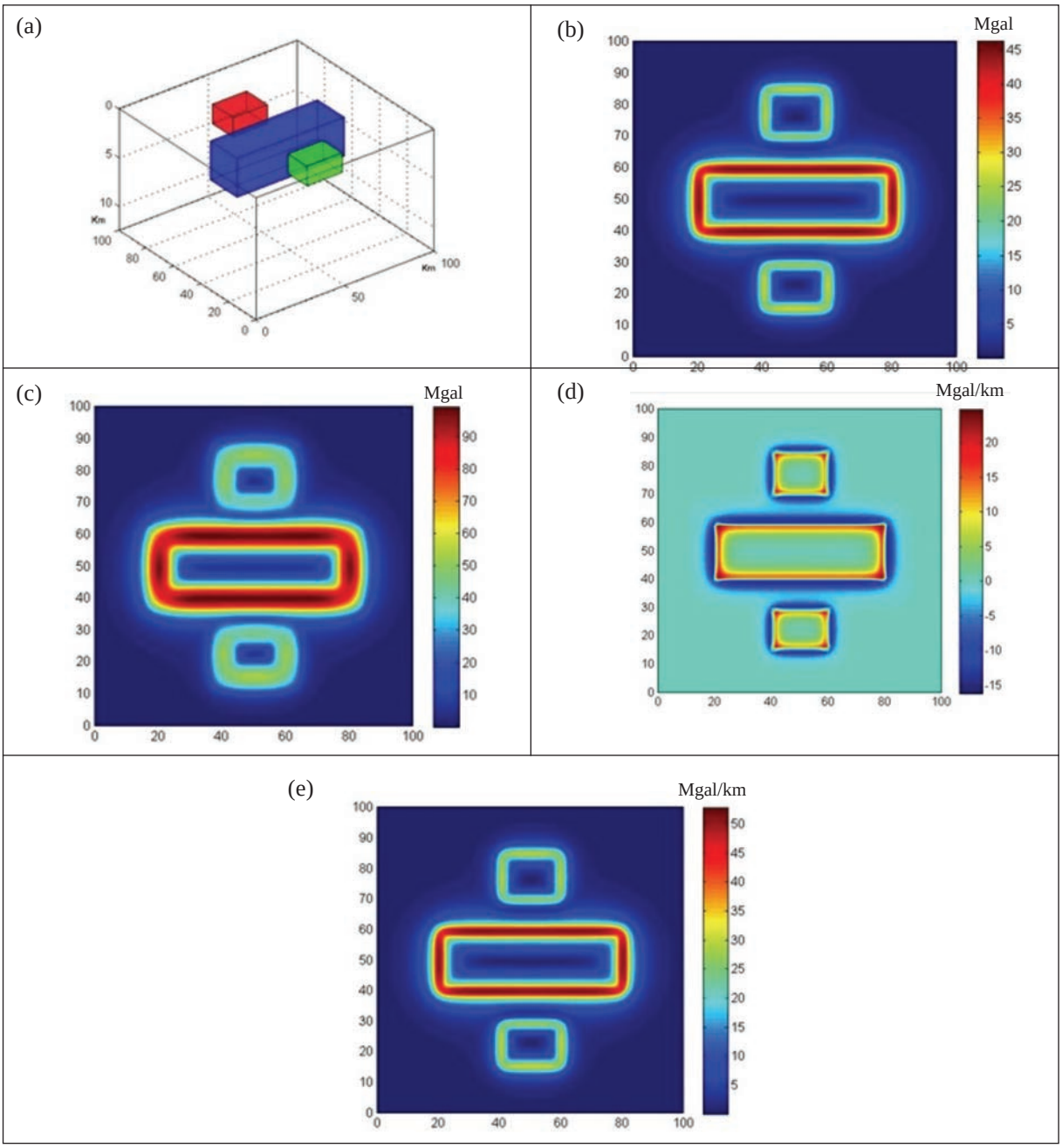

Figure 1- In order to compare the results of MSDVD, the responds of the multiple structures with different density and depth were used. The blue structure has a density of 2.7 gr/cm^3 at depth of 5 km, the red structure has a density of 2.5 gr/cm^3 at depth of 1 km and the green structure has a density of 2.9 gr/cm^3 at depth of 1 km (a). The responds are given for (3x3) dimensional filter in (b), (5x5) dimensional filter in (c), vertical derivative in (d) and horizontal derivative in (e).

In figure 2, the prisms with known depth and density of the Simav Graben are used. The thickening and condensing borders show an enhanced image of the prisms (Figure 2a). The amplitudes vary inversely proportional with the depth and the amplitude ratios are preserved (Figure 2b).

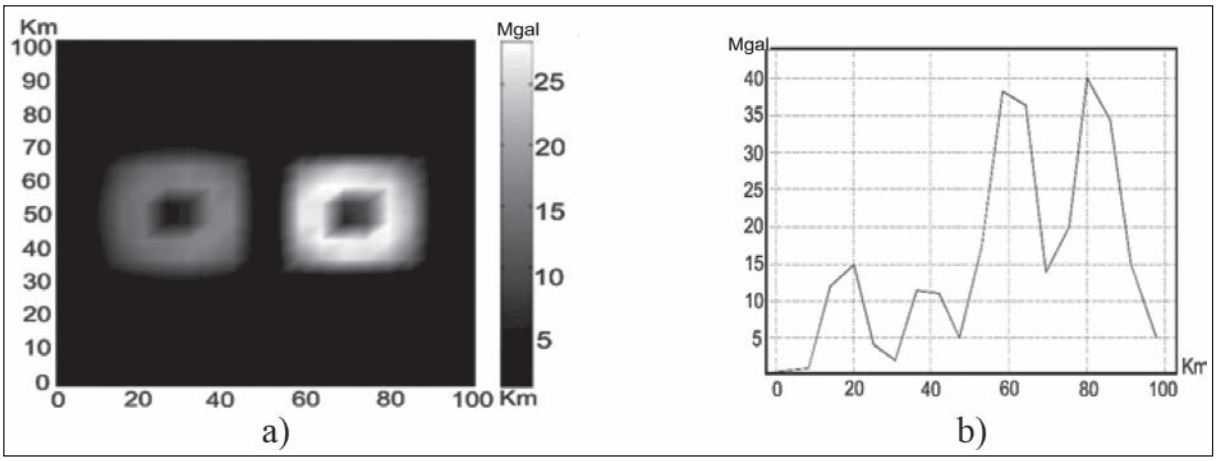

Figure 2- Selected dimensions and depths of prisms to see the effects on the graben scale: shallow prism (right) 20x20x1.2 km d=2.2 gr/cm^3 and deep prism (left) 20x20x13 km d=2.9 gr/cm^3. a) MSDVD result for the prisms, b) values along the center line crossing both prisms, the shallow prism gives a higher standard deviation value.

3. Geological Setting of the Study Area

The Aegean grabens, including the Simav Graben, have attracted investigators since 60's (Arpat and Bingöl, 1969). The E-W directional Pliocene?-Quaternary depression area restricted by the Simav Fault, which delimits the NE-SW directional Demirci, Selendi, Gördes basins in the north, is called as the Simav Graben (Şaroğlu, 2002). Seyitoğlu et al. (1997), from the resolutions of fault mechanism, stated that the Simav Fault was an active and listric fault. This structure is one of the latest products of N-S extensional tectonic, which affects the Aegean region in Late Oligocene-Early Miocene period (Seyitoğlu et al., 1997).

Geomorphological evidences point out that the plain in which the Simav Lake is located has been depressed by the earthquakes within last ten thousand years (Doğan and Emre, 2006). Another suggestion is that the Simav fault is 205 km long slip fault which is bounded to the Gelenbe fault zone in west and to the Sultandağı fault in east (Doğan and Emre, 2006). The northern border of the fault is limited by the Naşa Fault zone, which is formed by a set of normal faults, and the Emet (Kütahya) Fault Zone located in far north (Emre et al., 2012). According to Emre et al. (2012), the Simav plain, which is the largest structural depression that developed within the Simav Fault, is a basin that formed in right-stepping segment between the Simav and Şaphane faults. The regional map (Figure 3), shows the geology of the Simav and its vicinity, and the study area.

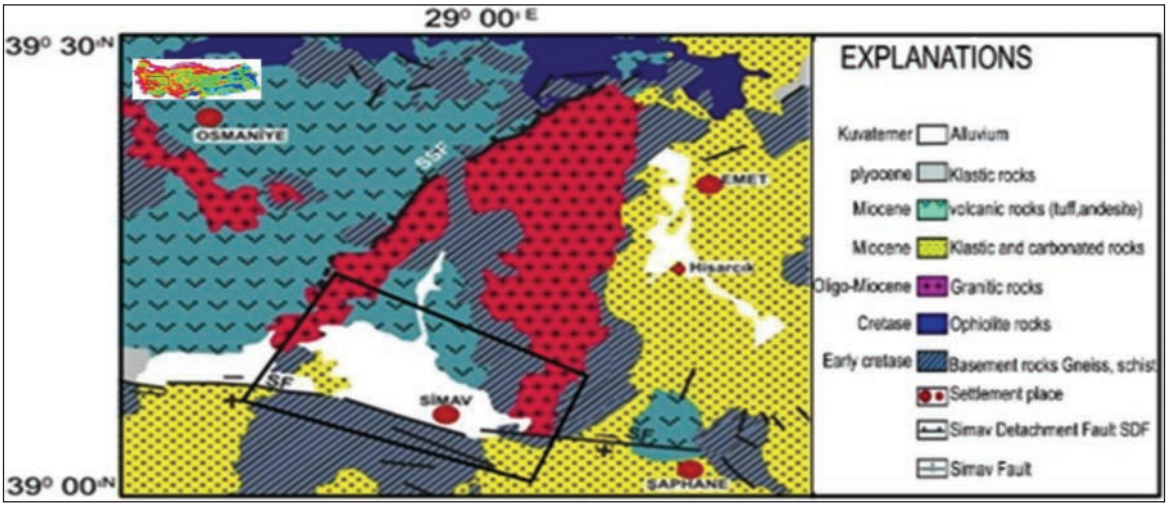

Figure 3- The geology of Simav and its vicinity (modified from MTA, 2002). Black square indicates the study area.

Emre et al. (2006) stated that the recent tectonic deformation, in which the earthquakes had occurred, was caused by the normal and strike slip faults. The investigators emphasize that the most significant earthquake epicenters are the NW-SE directional, right lateral Simav fault and the NW-SE directional Naşa Fault Zone consisting of a set of parallel faults (dipping towards southwest between 55°-65°). The debates on whether the Simav fault is a normal fault as stated by Seyitoğlu et al. (1997) or a right lateral strike slip fault as suggested by Emre et al. (2012) still continue today.

Gündoğdu et al. (2016), presented the offsets on river beds in the stream drainage network by conducting lineament analysis, and suggested that the Simav Fault had continued its strike slip movement even in recent times (Figure 3).

The Simav Graben, is a tectonic junction of which its upper surface has a triangular geometry in the region between the Simav Fault and the Naşa Fault zones (Emre et al., 2006). Its lower edge and tip extend in NW and SE directions, respectively.

The Simav fault in south of the Simav Graben is a NE dipping, steeply inclined with a decreasing slope as going deeper the form of semi-graben. This is also an asymmetrical semi-graben in which the antithetic normal faults developed with their roots extending to the Simav fault.

In the east of the Simav basin, the corner structure created by the intersection of the Simav fault and the Naşa Fault zone, (Figure 4, inside the white circle) is clearly observed in the data (Toker, 2014).

The presence of a third discontinuity (SW-NE directional) that cuts this intersection can be seen from the lineaments in the surface data. This discontinuity can also be traced on the three dimensional gravity depth interface (13-15 km) obtained by the iterative inverse solution method.

It is known that earthquakes occurred in the graben are associated with the characteristics of tectonic junction. The Simav fault bends and changes its direction within the Simav graben.

4. The Application of Methods to the Gravity Data

Data used in this study was measured by MTA in 1984. The gravity data, including base stations, were collected at 964 points. The station interval is approximately 250 m. The Bouguer density value was set as 2.67 gr/cm^3 and the Bouguer anomaly map was produced after routine processing steps (Demirbaş and Uslu, 1984). The shape and location of the graben can be traced on the gravity map (Figure 4). The data vary between -55 and -75 mGal (Figure 5b). In the gravity map, the value ranges between -60 and -64 mGal represent granitoids, and the values ranging between -72 and -74 mGal represent gneisses which extend along the lower edge of the graben (Toker, 2014). Blue areas in figure 5b present the gravity effect of the Quaternary alluvial fill. The area shown with white line in figures 5b, c, d and e is the subject of this study.

The results of 3x3-dimensional MSDVD application by setting k=1 and 9x9-dimensional MSDVD application by setting k=4 are shown in figures 5c and d, respectively.

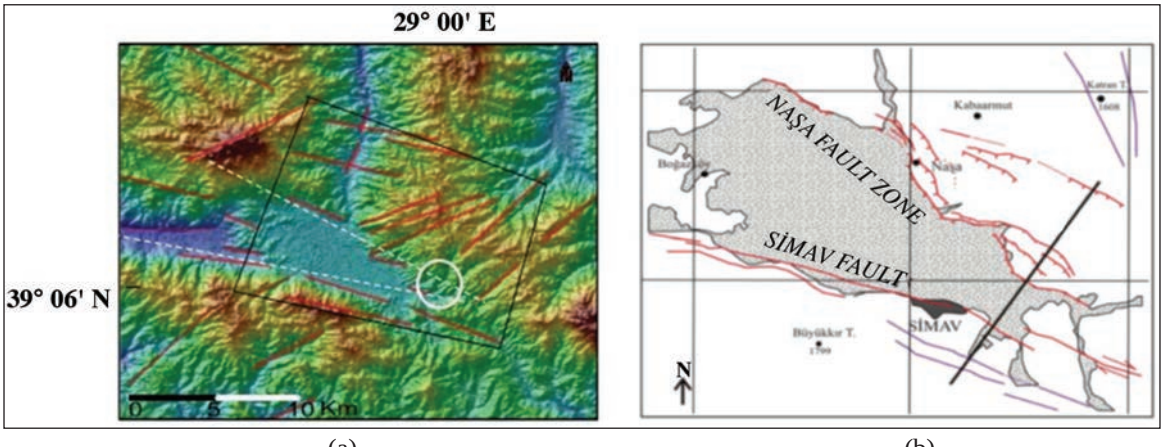

(a) (b)

Figure 4- a) Lineament analysis of Simav and its vicinity (white circle: corner structure, see text for explanation), b) active faults in the region (Emre et al., 2012).

The map shown in figure 5 c) appears to be simplified in figure 5 d) due to the reduced sensitivity. The map in figure 5 d) is composed of both graben itself and a circular intrusive structure that is forced into SW part of the graben.

The sun shading (Cooper and Cowan, 2003) technique was applied to the Bouguer data at a height of 500 m from SW (Figure 5e).

The relief map obtained from the standard 3D Euler Deconvolution is shown in figure 5f (Thompson, 1982; Reid et al., 1990).The target structure is marked with red dashed circle.

The gravity map has a high resolution and the conceptual model of the graben is supported by the data (Toker, 2014). The depth of the infill of the graben reaches 1200-1300 m in the model by means of two dimensional gravity inverse solution. This thickness

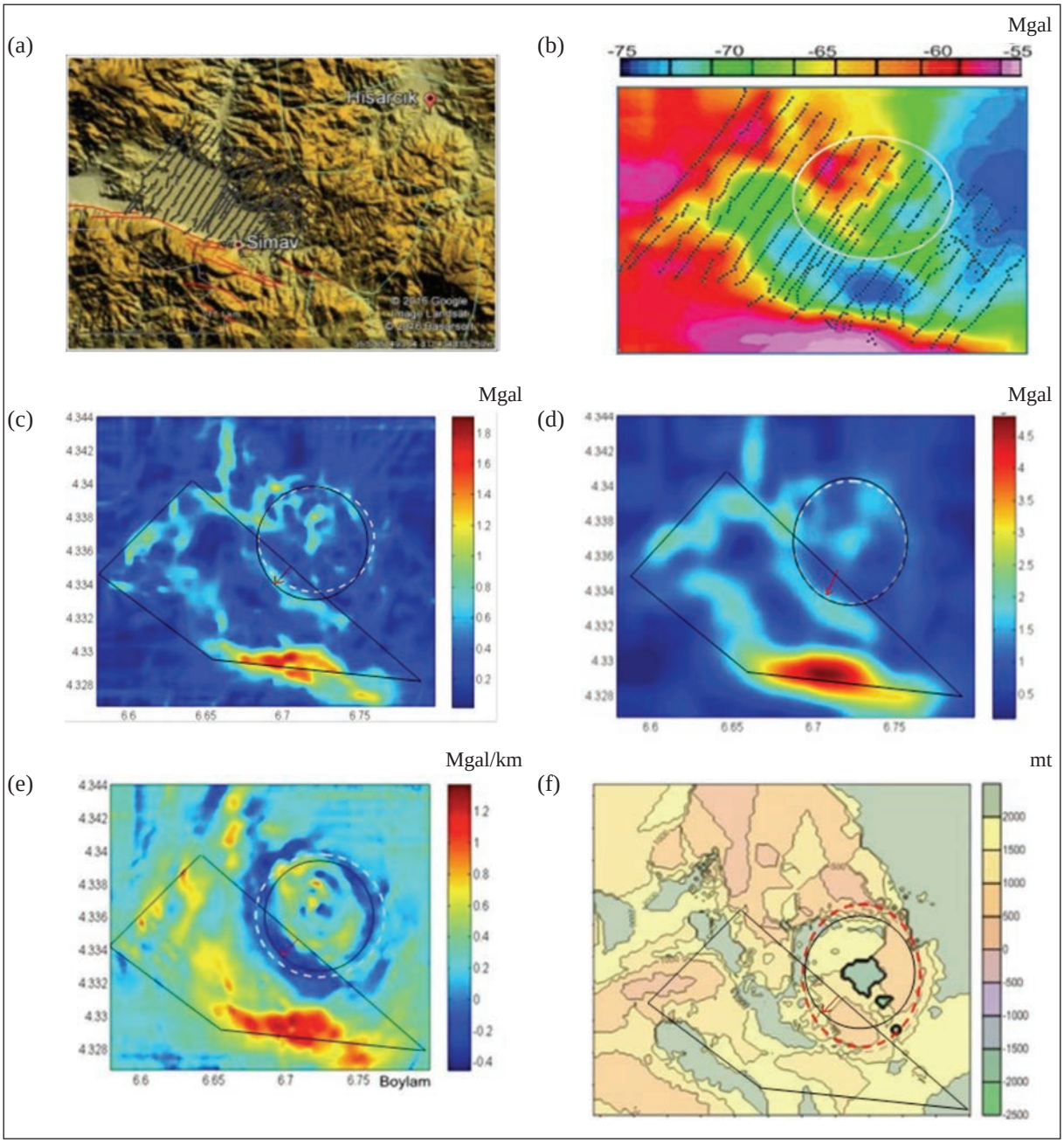

Figure 5- a) Study area, b) Bouguer map, c) MSDVD for k=1 (3x3), d) MSDVD for k=4 (9x9), e) 500 m. sun shading, f) Euler relief map (see text for details).

decreases towards northward and westward starting from the Simav settlement area (Toker, 2014).

The result of the three-dimensional modelling showed that the depth of the interface between the Simav fault and the Nasa Fault zones lies within a range of 13-15 km's, and the traces of a discontinuity in the GB - NE direction (Toker, 2014). With the reprocessing of the data, the information was obtained not only in terms of linearity and boundary relationships but also in terms of geological mass.

In edge detection analyses, the structural boundaries can be traced by using derivative and phase components.

Using a MSDVD filter with a 9x9 window size, the existence of a circular structure which emplaced in to 2/5 of the graben by forcing was revealed. The MSDVD filter exhibits positive features such as not having negative effects on the phase filter due to lacking of the oscillation caused by the vertical derivative (Toker et al., 2014) as well as strengthening the effect of geological structure.

The boundaries and the relief of this structure were investigated by the three-dimensional standard Euler deconvolution (Table 1). The structural index is 1 and the window size is 2219 x 2219 m. There is no altitude information. The depth is defined up to 20 times of the station interval.

To the north of the graben, it is observed that there is a root in the middle of this circular structure and this root extends downward deeper than 2 km (Figure 5f).

Within the frame of this study, a circular structure, which some researchers identified as the Roof Subsidence, is envisaged as intrusions with a diameter of about 9 km by locating its existence and geometry from geophysical data.

Table 1- 3d Euler Deconvolution parameters.

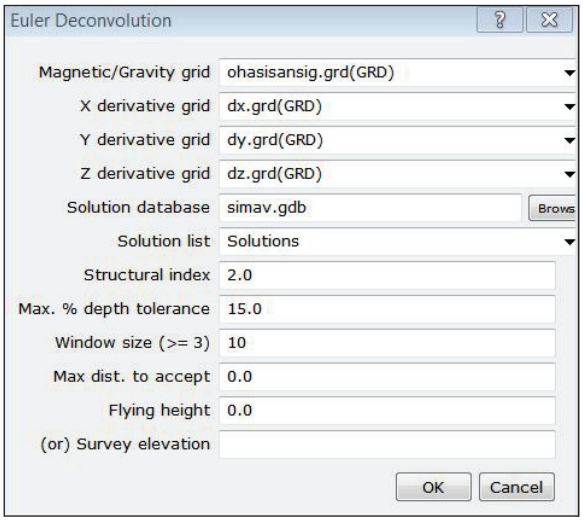

The study showed that the appropriate MSDVD size for this region is 9x9 in terms of lean imaging of the tectonic elements.

However; it should be kept in mind that these values are data and target dependent. When working in other areas, different size of filters should be tested and site specific filter dimensions should always be sought.

5. Seismological Activity

Approximately 1086 earthquake records were taken from Bogazici University Kandilli Observatory data base (www.koeri.boun.edu.tr / scripts / sondepremler.asp, 2016), and their distributions are shown in figure 6. The epicenters of earthquakes become dense around 5-10 km and their depths show a distribution down to 25 km (Figure 7).

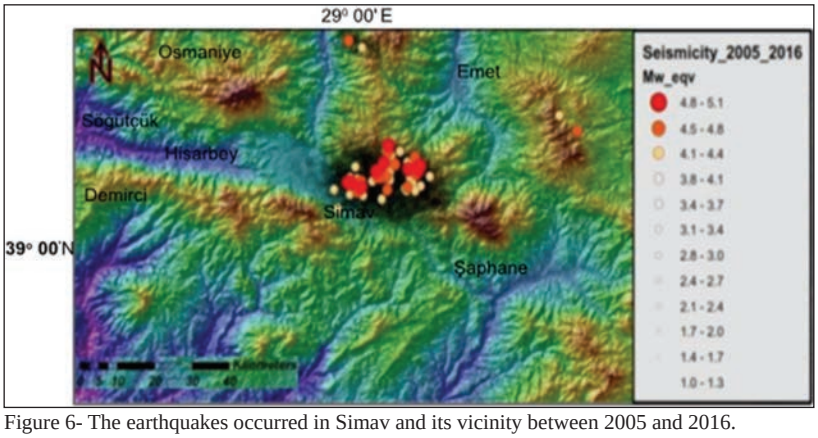

Figure 6- The earthquakes occurred in Simav and its vicinity between 2005 and 2016.

Kartal and Kadiroğlu (2014) examined 39 earthquakes magnitudes of which are greater than 4.0. The earthquakes are divided into two groups, SW and NE groups, at the area in the east of the proposed structure. Table 2 shows those related to the circular structure. The occurrence intervals of earthquakes on the chart are very short. Five of them occurred with one day interval and on the same circular structure.

The distribution geometry of the in hypocenter and epicenters of the earthquake is given in figure 7 as 3D. Figure 7 inset shows that there are two intrusions connected to each other in the region where the distribution of the hypocenters are concentrated. The image shows that the locations of the hypocenters related to the boundaries of the intrusion and that when these intrusion rise or change direction, these movements create small earthquakes.

Table 2- Earthquakes that occurred over the circular intrusion (Kartal and Kadiroğlu, 2014).

No	Date	Time (GMT)	Lat.	Lon.	Depth	MI	Direct1	Slope1	Angle1	Direc2	Slope2	Angle2
1	19.05.2011	20:15:22:79	39.1328	29.0820	24.46	5.7	149	35	-45	278	66	-117
4	19.05.2011	21:21:29:45	39.1128	29.0317	06.99	4.3	127	44	-68	278	50	-110
7	20.05.2011	00:58:33:05	39.1147	29.0837	17.38	4.3	84	26	-80	252	64	-95
9	20.05.2011	05:00:36.19	39.1202	29.0872	07.09	4.2	79	46	-79	243	45	-101
10	21.05.2011	21:43:08.56	39.1037	29.0513	07.00	4.0	302	43	-92	124	47	-89
11	24.05.2011	02:55:28.91	39.1013	29.0217	16.80	4.2	44	58	-87	219	32	-94
15	29.05.2011	01:31:39.16	39.1425	29.0853	05.04	4.5	129	37	-50	263	63	-116
19	27.06.2011	21:13:58.53	39.1108	29.0260	18.27	5.0	156	33	-65	307	60	-105
22	03.07.2011	14:16:28.51	39.1037	29.0147	10.78	4.1	159	47	-36	275	64	-131
34	03.05.2012	16:16:04.27	39.1018	29.0390	25.41	4.6	153	48	-60	292	50	-119

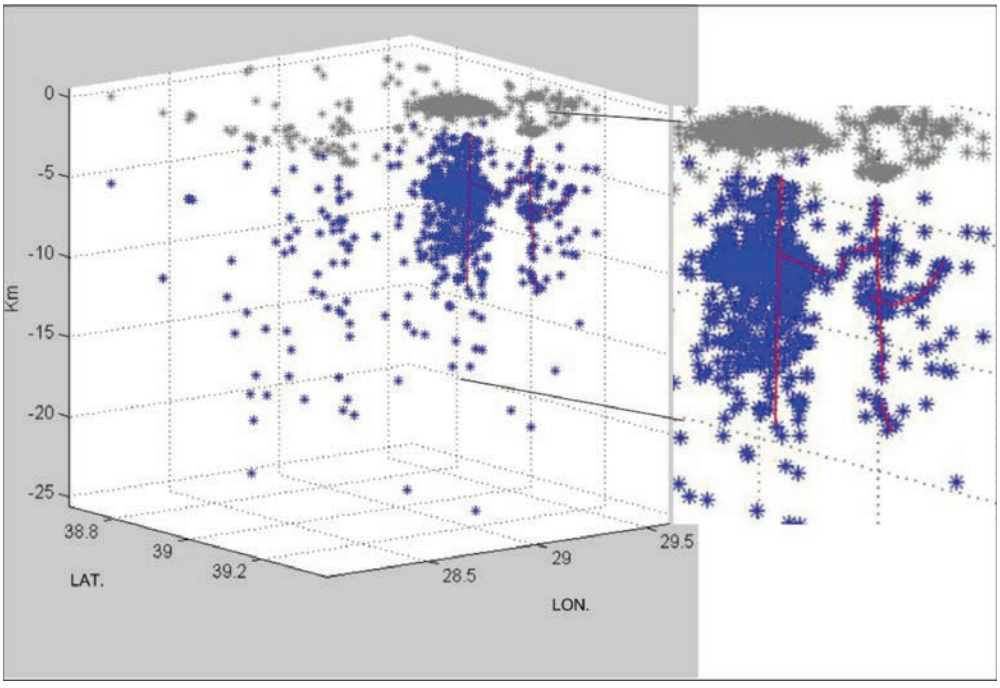

Figure 7- Distribution geometry (dark blue: hypocenter, gray: epicenter). Red lines indicate the probable structural relationship and nearly parallel the vertical axes (B.Ü. Kandilli Obsevatory catalog).

6. 3D Modelling of the Circular Structure

In order to make the depression area distinguishable in 2D depth map, cross sections were taken (Figure 8a). In these sections; there are seen circular structures in which sectional images of deep blue traps are located and the depth information belonging to those images. There are also observed columnar structures, which have traces of contours starting from the center of the circular structure to the right. Their depths rest on the boundary of the block diagram and are most probably continuous. It is considered that these are the structures, which are revealed by the monitoring of earthquake epicenters, and possess images that resemble to combined structures.

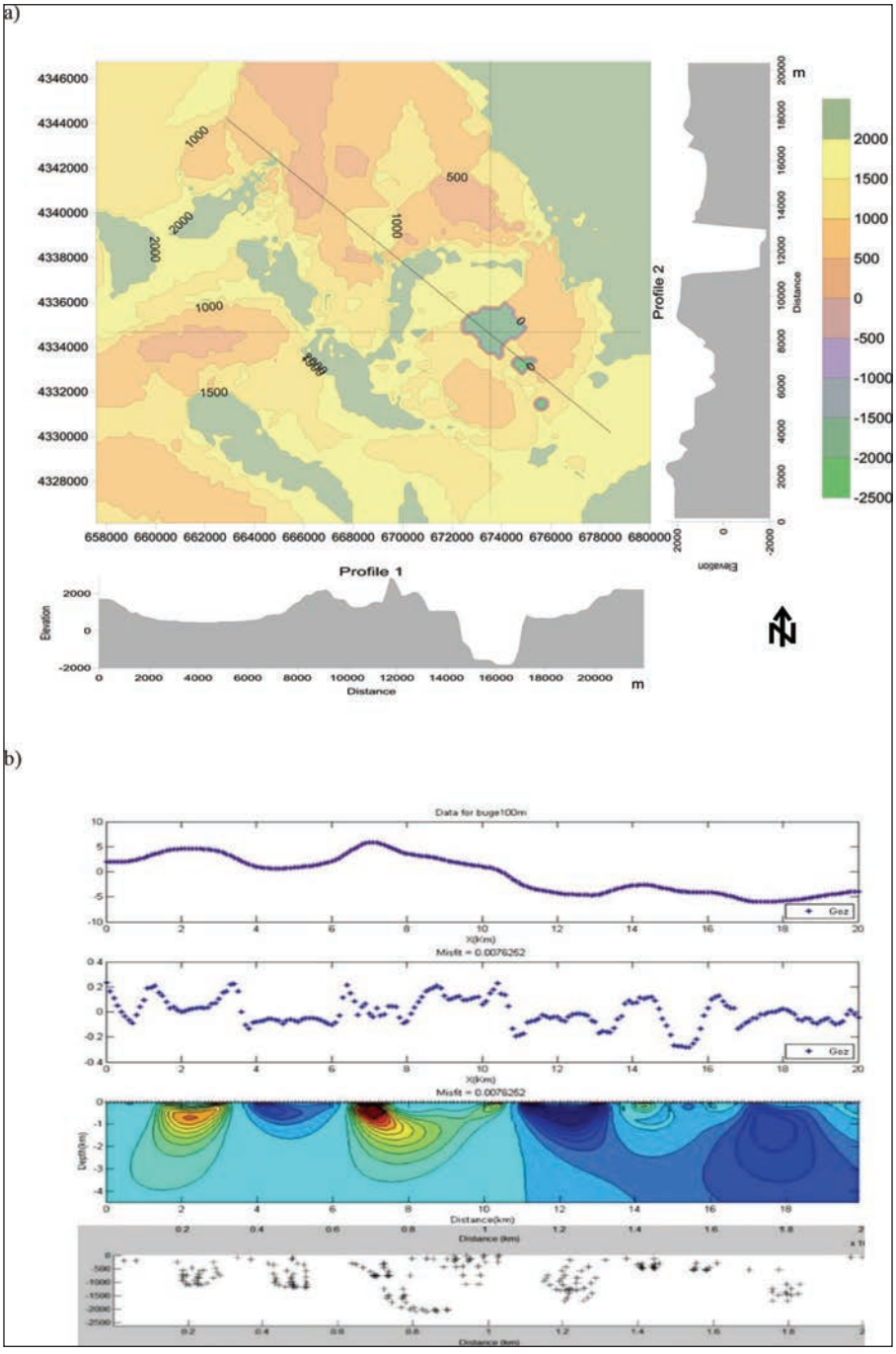

Figure 8- **a)** The bottom topography of the circular structure along the profiles, **b)** comparison of the results from 2D inverse solution and tilt depth method with horizontal cylinder approach**.**

In order to see the gravity distribution of the model in figure 8b, a model was generated by 2D inverse solution from the data taken along the brown colored line. The depth interval for 2D model was selected as 0-4.5 km by trials.

The presented density value makes differences with respect to 2670 kg/m^3. The incompatibility was detected as 0.0076624. In figure 8b, the result obtained by the tilt method is seen and the target structure between the distances of 4-6 km's was imaged as certain (Cooper, 2011). The depth comparison was not made.

Figure 9 shows a three-dimensional gravitational relief map obtained by the standard Euler Deconvolution method. The relief map clearly shows the Simav fault and the Naşa fault which surround the Simav half graben. Besides, the figure 9 also shows the presence and the depth of the circular structure in the northern part.

7. Discussion

The existence of a buried circular structure, which has not previously been revealed in the gravitational data, was investigated. When we were changed structural indice for dyke model (ı=2), relief has not been changing. Model was stable for both indices.

Here, with the weighing ability of the MSDVD filter to the structural information an image similar to

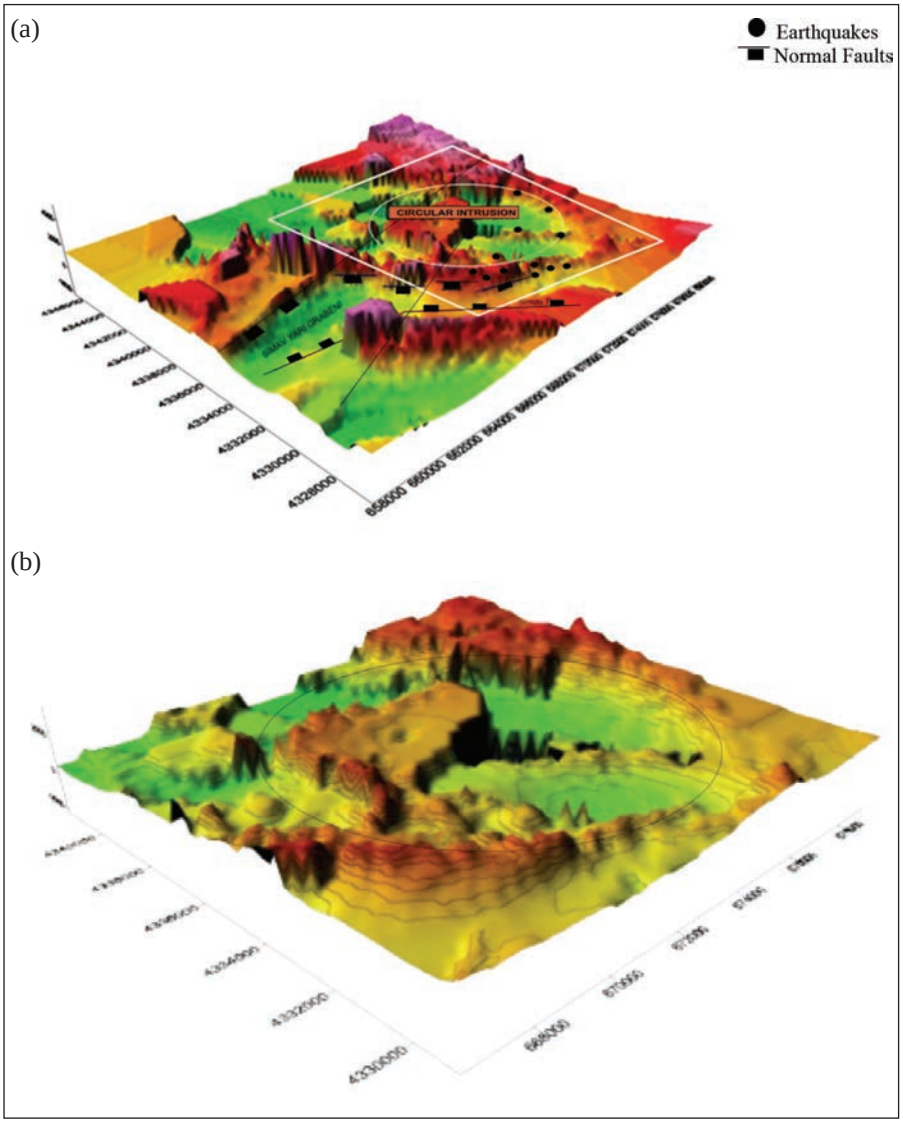

Figure 9- **a)** 3D relief image of the gravity data obtained from the 3D standard Euler deconvolution, **b)** The close-up view of the circular structure.

the horizontal derivative was obtained without using derivative and phase filter.

The MSDVD was used to illuminate structure-boundary relationships. The experiments performed in this work showed that an operator with a size of 9x9 was appropriate for this field. It should not be forgotten that these values will change when working in different regions.

Before applying the real data, testing on synthetic data and supporting with modeling exercises is the most appropriate way to select the operator size.

The circular structure suggested in this study is connected to earthquakes down to 25 km in depth and triggered these earthquakes.

In the previous study, the intersecting discontinuities in the graben were revealed (Toker, 2014).

In this study, it is thought that the junction of discontinuities creates a weak zone where magmatic melt easily and rapidly ascends, and mobilizes the circular structure.

As a result, it is thought that magmatic melt migrates through weak geological zones (contact, faults, etc.) and creates new pathways for itself.

It is also thought that earthquakes that occurred in the region is due to the location of the circular structure (29.00E longitude 39.10N latitude).

The surface traces of these earthquakes need to be investigated with respect to the location of the circular structure. In addition, an additional geophysical work is needed in this area. The investigation of acoustic, resistivity and magnetic susceptibility parameters will help resolve the problem.

8. Result and Suggestions

Basically, three cases can be count on the earthquakes that occur in the region. Earthquakes created by,

- The intersection zone where the Simav Fault, the Naşa Fault and the deep seated SW-NE directional discontinuity cross each other,

- The presence of a structure of intrusions rising at the junction of these discontinuities,

- The corporate work of both conditions given above.

In this work, the gravity data were reprocessed and modelled to reveal the existence of a tectonic junction and intrusive structure with circular geometry. This intrusion is the result of horizontal and vertical tectonic activities of the region.

It is concluded that earthquakes, which occurred in the region, are caused by these intrusions and the tectonic junction formed by the active faults.

If the area among three settlements is to be used as a living area, the necessary measures for the building safety must be taken into consideration. It is believed that this area has a priority in terms of preventing future inconveniences.

Acknowledgements

Data utilized in this study belong to the General Directorate of Mineral Research and Exploration (MTA) and was published with the written permission of the organization. We are thankful to MTA for their supports. The software was implemented from D'errico (2016). F. Alkan Tetik and Recep Çakır contributed to this article with their valuable opinions and suggestions. We also would like to thank to referees for their critics and constructive suggestions.

References

Ansari, A. H., Alamdar, K. 2011. A new edge detection method based on the analytic signal of tilt angle (ASTA) for magnetic and gravity anomalies, IJST A2: 81-88, Iranian Journal of Science and Technology.

Arısoy, M.Ö., Dikmen, Ü. 2011. Potensoft: MATLAB based software for potential field data processing, modeling and mapping, Computer And Geoscience, 37, 7, s. 935 – 942.

Arpat, E., Bingöl, E. 1969. Ege bölgesi graben sisteminin gelişimi üzerine düşünceler, Maden Tetkik ve Arama Dergisi, 73, 1-9, Ankara.

Bekler, T., Demirci, A., Özden, S., Kalafat, D. 2011. Simav, Emet fay zonlarındaki optimum kaynak parametrelerinin analizi, 1. Türkiye Deprem Mühendisliği ve Sismoloji Konferansı, ODTÜ, Ankara.

Boğaziçi Üniversitesi Kandilli Rasathanesi Deprem Kataloğu. 2016. www.koeri.boun.edu.tr/scripts/sondepremler.asp

Cooper, G.R.J., 2011. The Semi-Automatic Interpretation of Gravity Profile Data March 2011, Computers and Geosciences 37(8) DOI: 10.1016/j.cageo.2011.02.016.

Cooper, G. R. J. 2013. Reply to "A Discussion about the Hyperbolic Tilt Angle Method by Zhou et al.", Computers and Geosciences, 52, 496-497.

Cooper, G.R.J., Cowan, D.R. 2003. Sunshading geophysical data using fractional order horizontal gradients. The Leading Edge. 22:204

Cooper, G.R.J., Cowan, D.R. 2004. Filtering using variable order vertical derivatives. Computer and Geoscience, 30, 455-459.

Demirbaş, Ş., Uslu A. 1984. Kütahya Simav Gravite Etüdü, Maden Tetkik ve Arama Genel Müdürlüğü Rapor No: 8136, Ankara (unpublished).

D'errico, J. 2016. Personel Web Page https://www.mathworks.com/matlabcentral/.../869215-john-

Doğan, A., Emre, Ö. 2006. Ege graben sisteminin kuzey sınırı: Sındırgı Sincanlı Fay Zonu, 59. Türkiye Jeoloji Kurultayı, Bildiriler Kitabı.

Emre, Ö., Duman, T.Y., Olgun, Ş., Özalp, S. 2012. Türkiye diri fay haritası (renwed), Maden Tetkik ve Arama Yayınları, Ankara.

Doğan, A., Emre, Ö. 2006. Ege graben sisteminin kuzey sınırı: Sındırgı Sincanlı Fay Zonu, 59. Türkiye Jeoloji Kurultayı, Bildiriler Kitabı.

Gündoğdu, E., Özden, S., Karaca, Ö. 2016. Comparative structural analysis of field data from Simav fault and surrounding area with alos-palsar and landsat images, Journal of the graduate school of natural and applied sciences of Erciyes University Vol :32 No:1

Hsu, S.K., Sibuet, J.C., Shyu, C.T. 1996. Depth to magnetic source using generalized analytic signal,Geophysics, 61, 373-386.

Jassim, F.A. 2013. Semi – optimal edge detector based on simple standard deviation with adjusted thresholding, International Journal of Computer Applications (0975 – 8887) Volume 68– No.2, April 2013.

Kartal, R.F., Kadiroğlu, F.T. 2014. 2011-2012 Simav Earthquakes (Ml=5.7, Ml=5.0, Ml=5.4) and Relationship with the Tectonic Structure of the Region Yerbilimleri, Bulletin of the Earth Sciences Application and Research Centre of Hacettepe University 35 (3), 185-198.

MTA 2002. General Directorate of Mineral Research and Exploration. http://www.mta.gov.tr/v30/hizmetler/500cd.

Miller, H. G., Sing, V. 1994. Potential field tilt - A new concept for location of potential field sources Journal of Applied Geophysics, 32, 213-217

Oasis montaj Sofware, 2009 www.geosoft.com/resources/goto/oasis-montaj-7.1 Queens Quay Terminal 207 Queens Quay West Suite 810, PO Box 131 Toronto, ON Canada M5J 1A7

Reid, A. B., Allsop, J. M., Granser, H., Millett, A. J., Somerton, I. W. 1990. Magnetic interpretation in three dimensions using Euler deconvolution, Geophysics, 55, 80–91, http://dx.doi.org/10.1190/1.1442774

Seyitoğlu, G. 1997. The Simav Graben: An example of young E-W trending structures in the late cenosoic extensional system of western Turkey. Turkish Journal of Earth Science, 6, 135-141, TÜBİTAK, Turkey.

Toker, C. E. 2014. Geophysical analysis and modelling of the Simav basin, Western Anatolia. Bulletin of the Mineral Research and Exploration. 148, 119-135, Ankara.

Toker, C. E., Çiftçi, Y., Ayva, A., Kürçer, A. 2014. Two examples for imaging buried geological boundaries: Sinkhole structure and Seyit Hacı fault, Karapınar, Konya. Bulletin of the Mineral Research and Exploration. 149, 189-199, Ankara.

Thompson, D. T. 1982. EULDPH: A new technique for making computer-assisted depth estimates from magnetic data, Geophysics, 47, 31–37, http://dx.doi.org/10.1190/1.1441278

Verdusco, B., Fairhead, J.D., Green, C.M. 2004. New insigth in to magnetic derivatives for structural mapping, Leading Edge, 23 (2), 116-119.

Zhou, W., Do, X., Li, J. 2013. A Discussion about hyperbolic tilt angle method, Computer and Geoscience, V. 52, p. 493-495.